Ore Geology Reviews 64 (2015) 89–102

Contents lists available at ScienceDirect

Ore Geology Reviews

journal homepage: www.elsevier.com/locate/oregeorev

Significant Zn–Pb–Cu remobilization of a syngenetic stratabound deposit during regional metamorphism: A case study in the giant Dongshengmiao deposit, northern China

Richen Zhong [a,b], Wenbo Li [b,*], Yanjing Chen [b], Jianqing Ji [b], Yongfei Yang [b], Chuansheng Hu [b]

[a] Civil and Environmental Engineering School, University of Science and Technology Beijing, Beijing 100083, China
[b] The Key Laboratory of Orogenic Belts and Crustal Evolution, School of Earth and Space Sciences, Peking University, Beijing 100871, China

ARTICLE INFO

Article history:
Received 3 April 2014
Received in revised form 17 June 2014
Accepted 17 June 2014
Available online 24 June 2014

Keywords:
Zn–Pb–Cu remobilization
Petrography
$^{39}Ar/^{40}Ar$ geochronology
Intraplate orogenic belt

ABSTRACT

The giant Dongshengmiao Zn–Pb–Cu deposit is located in the Langshan district, northern China. The ores are hosted within a Proterozoic rift sequence, which underwent lower greenschist facies metamorphism and shear deformation during development of Early Cretaceous intraplate orogenic belt. Northwest-dipping thrust faults, which share similar orientations and dip angles with the orebodies, are well developed in the mining area. Syngenetic stratabound sulfides were formed during the Proterozoic rifting event, but syngenetic ore textures have seldom been preserved except for some pretectonic fine-grained pyrite. Petrological observation, $^{39}Ar/^{40}Ar$ geochronology, combined with previous isotopic and fluid inclusion studies indicates that significant Zn–Pb–Cu remobilization took place as a result of thrust faulting associated with metamorphic devolatilization of ore-hosting rocks at ca. 136 Ma, coeval with the intraplate orogeny and regional crustal shortening. Sulfides were redistributed in shear structures or along grain boundaries of ore-hosting carbonates, and Fe-rich carbonates were ideal sites for Zn–Pb–Cu precipitation.

1. Introduction

The Langshan district in the western part of Inner Mongolia in northern China hosts a famous Cu–Pb–Zn polymetallic ore belt, and the Dongshengmiao Zn–Pb–Cu deposit is one of the largest tonnages and most representative deposits in the ore belt. Cu–Pb–Zn deposits in this ore belt are mostly hosted in greenschist to amphibolite facies Proterozoic rift sequences. These deposits have traditionally been related to submarine hydrothermal activity during development of the Proterozoic rift. Although it is widely accepted that these deposits underwent some degree of deformation and remobilization during Phanerozoic regional metamorphism or magmatic activity, the importance of epigenetic hydrothermal activity in shaping the present form of these deposits might have been underestimated by previous researchers. Our recent studies have shown that the Huogeqi, as another famous Cu–Pb–Zn deposit in this area, was deposited from metamorphic fluids during the activity of a shear zone (Zhong et al., 2012, 2013).

The genesis of the Dongshengmiao deposit is highly controversial as well, and two distinct genetic models have been proposed. A syngenetic model stresses that the Dongshengmiao Zn–Pb–Cu deposit is a metamorphosed sedimentary exhalative (SEDEX) ore system (Huang et al., 2001; Peng and Zhai, 2004; Peng et al., 2000, 2007b; Rui et al., 1994; Zhai et al., 2008). This model is mainly based on the geological settings of the deposit, such as host rift sequence, the presence of siderite layers and abundant massive pyrite, and the occurrence of B, Mn, P, Ba enrichments in some layers of the host rocks (Peng and Zhai, 2004; Peng et al., 2000, 2007a, 2007b; Yang, 1992; Zhai et al., 2008). During the development of the ore-hosting rift, submarine volcanic activity was manifested by the presence of intercalated bimodal volcanic rocks within the rift sequences, and this is a favorable geological setting for submarine hydrothermal mineralization (Peng and Zhai, 1997).

However, macroscopic and mesoscopic structural observations revealed substantial evidences of structurally controlled mineralization, and an alternative genetic model was proposed, stressing that mineralization was controlled by thrust faults and that the metals were precipitated from syn-deformation epigenetic fluids (Niu et al., 1991; Sun and Niu, 1994). More recently, a multistage genetic model was proposed to account for the mixed syngenetic and epigenetic characteristics of this deposit. Based mainly on textures and REE geochemistry of ores, Zhang et al. (2010b) proposed that S-rich orebodies in the Dongshengmiao were formed by submarine exhalation, whereas Zn–Pb–Cu orebodies were precipitated from epigenetic hydrothermal fluids. Peng et al. (2007a) showed that some disconcordant vein-type Zn–Pb–Cu ores show characteristics of epigenetic hydrothermal mineralization and locally replace pyrite crystals, indicating a multistage mineralization of the Dongshengmiao deposit.

* Corresponding author.
E-mail address: liwenbo@pku.edu.cn (W. Li).

http://dx.doi.org/10.1016/j.oregeorev.2014.06.015
0169-1368/

Discrimination between metamorphosed and metamorphogenic deposit in metamorphic terranes is always a challenge (Marshall et al., 2000). For deposits hosted in metamorphic rocks, detailed and systematic microscope observations of ore and host rock textural relationships are an effective tool to reveal the relative timing between mineralization, host rock metamorphism, and deformation (Cartwright and Oliver, 2000; Marshall et al., 2000). A detailed petrographic study was carried out, in order to characterize host rock deformation and metamorphism, the relative timing of massive pyrite formation and Zn–Pb–Cu mineralization, and the pressure–temperature (P–T) conditions of the Zn–Pb–Cu mineralization and host rock deformation and metamorphism. The sphalerite geobarometer was also used to reveal the crustal depth of Zn–Pb–Cu mineralization and it yields consistent result with the petrologic observations. A systematic geochronological study was also carried out to provide further constraints on the genesis of the deposit and the tectonic background during ore-formation. The difference between massive pyrite and Zn–Pb–Cu ores is reviewed. At last, the Pb isotopic data of sulfides are compiled to trace the source of ore-forming metals. Based on this new information, a multistage genetic model is proposed, accounting for both macroscopic and microscopic characteristics of this deposit, and taking into account the body of geochemical and geochronological information.

2. Regional geology of the Langshan district

2.1. Pre-Mesozoic evolution

The Dongshengmiao deposit is located in the Langshan district, which is in the northwest corner of the Ordos Plateau, northern China (Fig. 1). Here, an Archean high-grade metamorphic complex is locally exposed and forms the basement of the North China block (Fig. 2). This Archean basement is overlain by a Proterozoic rift sequence (Fig. 2), characterized by greenschist–amphibolite facies metamorphosed carbonates and clastic rocks, with interlayers of volcanic rocks (Zhai et al., 2008). The depositional age of the Proterozoic rift sequence was obtained from intercalated metavolcanic rocks dated at ca. 1750 Ma (single zircon U–Pb age; Li et al., 2007) and 1805 ± 76 Ma (whole rock Sm–Nd model age; Peng and Zhai, 1997). More recently, the depositional age of Proterozoic metasedimentary rocks was constrained to be younger than 1426 Ma by U–Pb dating on detrital zircons separated from Proterozoic quartzite (Sun et al., 2013), which is an age of Mesoproterozoic. Neoproterozoic volcanic rocks are also reported in outcrops near the Tanyaokou deposit (Fig. 2). These volcanic rocks yield zircon U–Pb ages between 805 ± 5 Ma and 867 ± 10 Ma, and are interpreted to have erupted during a rifting event as well (Peng et al., 2010). It is not clear whether the Neoproterozoic volcanic rocks were originally deposited or were tectonically juxtaposed, and its relationship with the latest Paleoproterozoic–Mesoproterozoic rift also remains ambiguous.

Paleozoic sediments rarely occur in this area, except for some Carboniferous–Permian marine strata (Fig. 2), although contemporaneous intrusive rocks are abundant. The predominant Pre-Mesozoic intrusive rocks in the Langshan district are Late Paleozoic granite, granodiorite and intermediate rocks (Fig. 2), mostly dated at Late Carboniferous to Early Permian (Han et al., 2010; Pi et al., 2010). Some researchers proposed that final closure of the paleo-Asian ocean took place along the Suolon suture at the end of the Permian, resulting in amalgamation of the Mongolian Arcs and the North China Block (Fig. 1; Xiao et al., 2003; Zhang et al., 2009b, 2010a). Consequently the Late Paleozoic intrusive rocks were interpreted as formed in an Andean-like continental arc in the northern margin of the North China block, resulting from the southward subduction of the paleo-Asian ocean plate (Zhang et al., 2009b, 2010a). On the other hand, an alternative model proposed that the final closure of the paleo-Asian ocean was earlier than Late Devonian, and the Late Paleozoic plutons were formed in a post collisional tectonic setting (e.g., Xu et al., 2013). Besides, minor Proterozoic and Early Paleozoic granitoids are locally exposed in the Langshan district (Fig. 2).

2.2. Late Jurassic–Early Cretaceous intraplate orogeny

During the Late Jurassic–Early Cretaceous, intraplate deformations took place in a large area in Central and Eastern Asia, including Central Asia, southern Siberia, Mongolia and northern China (Dong et al., 2008; Yakubchuk, 2004). Although the geodynamic background is not well understood, far-field interaction of several convergent tectonic systems might have resulted in this intraplate deformation even, i.e. the southward propagation of the Siberia Craton in conjunction with the opening of the Amerasian basin; final closure of Mongol–Okhotsk

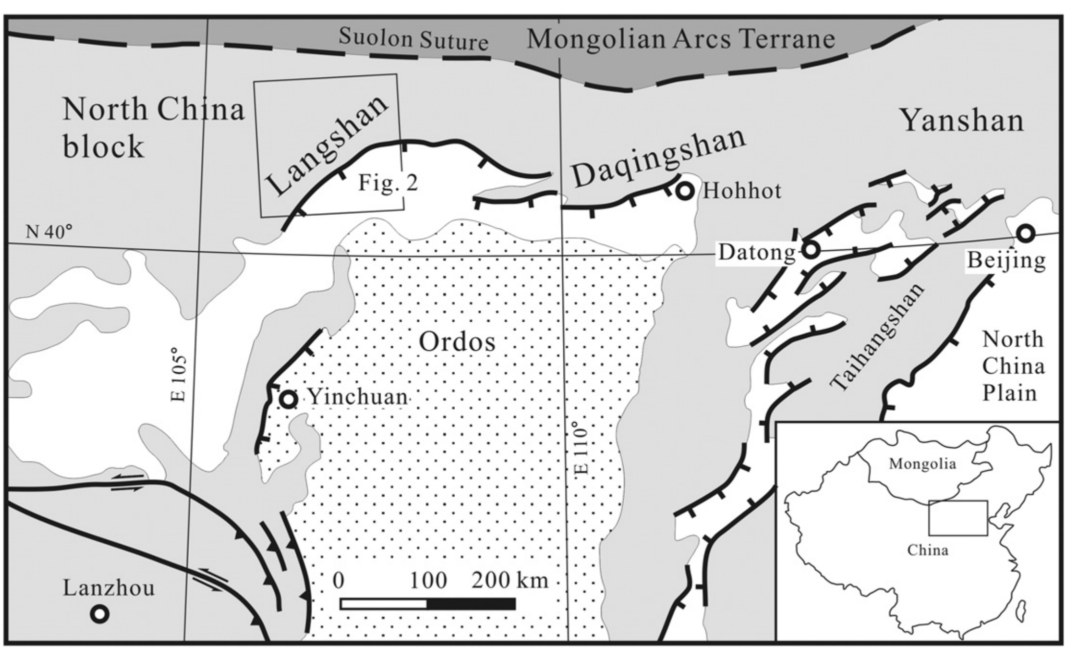

Fig. 1. Location map of the northern Ordos region, northern China. Dark gray, Mongolia Arcs terrane; light gray, North China block; stippled pattern, Ordos plateau (modified after Darby and Ritts, 2007).

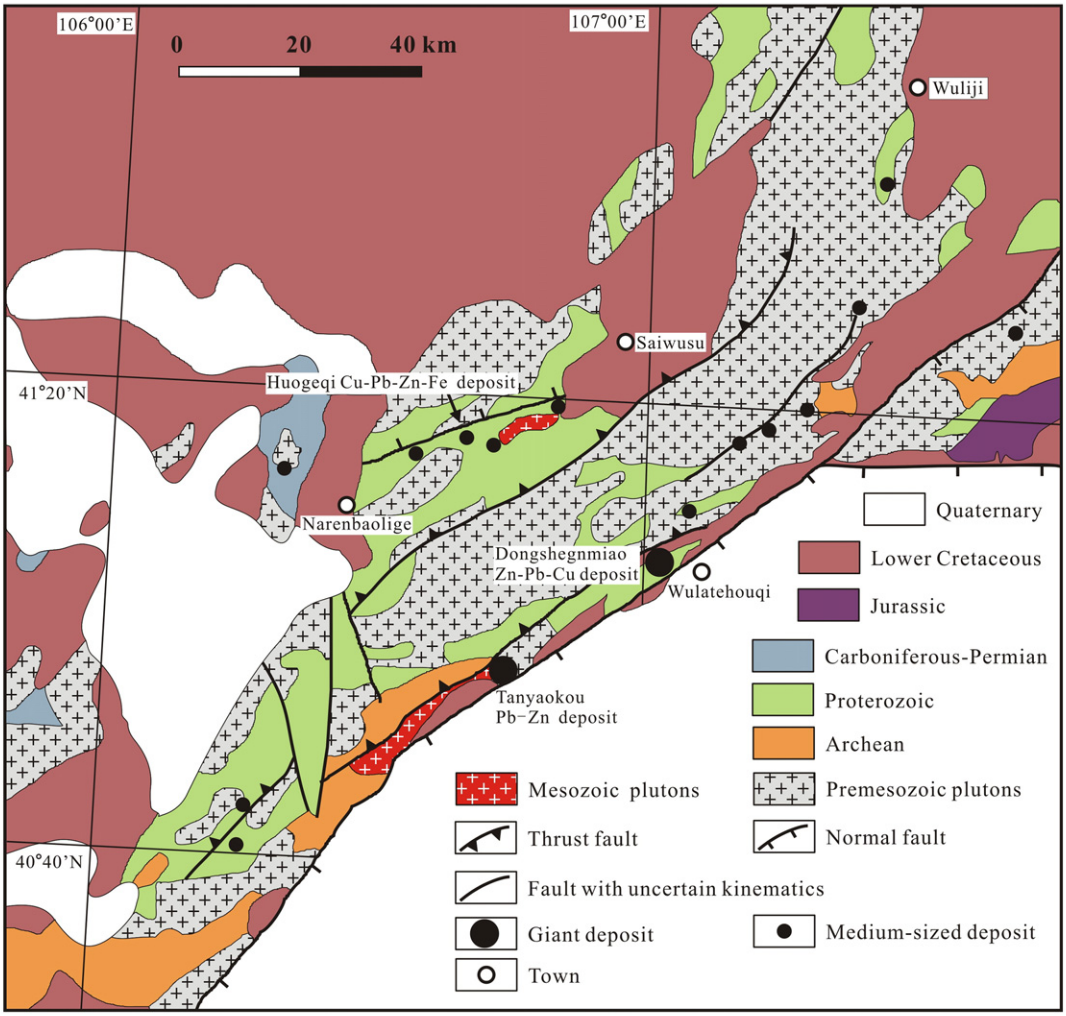

Fig. 2. Regional geology of the Langshan district (modified after Peng et al., 2007b).

Oceans; subduction of Pacific beneath Eurasian plates; and collision between the Lhasa and Qiangtang blocks (Darby and Ritts, 2007; Davis et al., 1998; Dong et al., 2008; Xu et al., 2001; Yakubchuk, 2004; Zheng et al., 1998).

The pattern of deformation varies in different areas. Large-scale strike-slip faults with offsets of several hundreds of kilometers are developed in Central Asia, Mongolia, and northeast China (Yakubchuk, 2004). Metamorphic core complexes and contemporary magmatic activities are locally observed in Daqinshan (Fig. 1; Davis and Darby, 2010; Qi et al., 2007; Wang et al., 2004) and eastern Mongolia (Daoudene et al., 2013). Large-scale thrust faults and related molasse-filled basins are developed in a 1200 km-long east–west-trending intraplate orogenic belt in northern China, known as Yanshan in the east and Daqingshan in the west (Fig. 1; Davis et al., 1998; Dong et al., 2008; He et al., 1998; Zhang et al., 2009a; Zheng et al., 1998). Accompanying the development of intraplate orogeny and the activity of thrust faults, regional metamorphism locally took place in this belt (Dong et al., 2008).

The Langshan district, which can be regarded as the southwestern continuation of the intraplate orogeny in the Daqingshan district (Fig. 1), is characterized by the development of northwest-dipping thrust faults and contemporaneous terrestrial sedimentary basins (Darby and Ritts, 2007; Gao, 2010; Li and Liu, 2009). Darby and Ritts (2007) proposed two phases of Late Jurassic–Early Cretaceous tectonism in the Langshan district: (1) a Late Jurassic–Early Cretaceous northwest–southeast crustal shortening, with development of thrust faults and widespread foreland basin sedimentation, followed by (2) a Late Cretaceous east–west extension, with development of a 12 km^2 basin bordered by normal faults. Most of the widespread Lower Cretaceous rocks in this area (Fig. 2) are interpreted as foreland basin sediments that formed during crustal shortening (Darby and Ritts, 2007). Combined with the widespread northwest-dipping Late Jurassic–Early Cretaceous thrust faults (Darby and Ritts, 2007; Gao, 2010; Li and Liu, 2009; Fig. 2) and the absence of metamorphic core complexes in the Langshan district, the deformation during convergence seems to have been much stronger than the subsequent regional extension.

2.3. Mineralization in the Langshan district

The giant (>2 Mt Cu, 1 Mt Pb and 1.7 Mt Zn; Singer, 1995) Dongshengmiao deposit, and more than ten medium-sized (0.06–2 Mt Cu, 0.07–1 Mt Pb and 0.11–1.7 Mt Zn; Singer, 1995) Cu–Pb–Zn polymetallic deposits, such as the Huogeqi Cu–Pb–Zn and the Tanyaokou Pb–Zn, occur in the Langshan district (Fig. 2). Most of these ore deposits are hosted by greenschist–amphibolite facies Proterozoic rift rocks and are distributed along northeast-trending faults (Fig. 2).

3. Geology of the Dongshengmiao deposit

Lithologies exposed in the mining area include Archean upper amphibolite–granulite facies rocks, lower greenschist facies Proterozoic rift sequence rocks, and unmetamorphosed Early Cretaceous foreland basin sediments related to intraplate orogeny (Figs. 3, 4). In the mining area the Archean rocks are mainly gneisses (Fig. 5A, B) and migmatites.

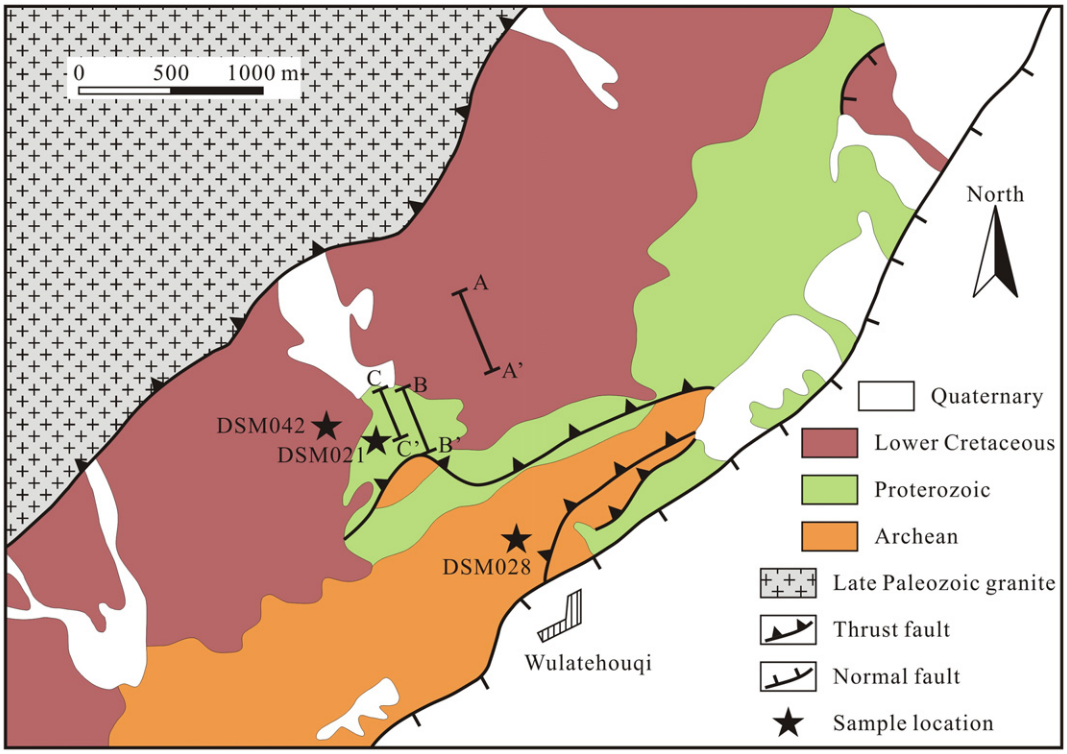

Fig. 3. Geological map of the Dongshengmiao ore deposit (modified after Zhai et al., 2008).

These high grade metamorphic rocks were previously regarded as the lower part of the Proterozoic sequence (Huang et al., 2001; Rui et al., 1994; Wulatehouqi Zijin Mining Group Co. Ltd, 2008; Zhai et al., 2008), but our unpublished zircon U–Pb SHRIMP study on migmatite yields a migmatisation (peak metamorphism) age of 2509 ± 35 Ma (MSWD = 3.8; n = 16), suggesting that they are Archean. Predominant lithological units of the ore-hosting lower greenschist facies Proterozoic rocks in the mining area include mica schist (Fig. 5C, D), quartzite (Fig. 5E), carbonaceous shale, dolomitic marble, intercalated basaltic and felsic metavolcanics (Peng and Zhai, 1997; Zhai et al., 2008), and siderite layers (Peng et al., 2000). The Proterozoic sequence is separated from the Archean rocks by northwest-dipping thrust faults along its southeast margin (Fig. 3). Early Cretaceous red sandstone, conglomerate and mudstone rest unconformably on the Precambrian metamorphic

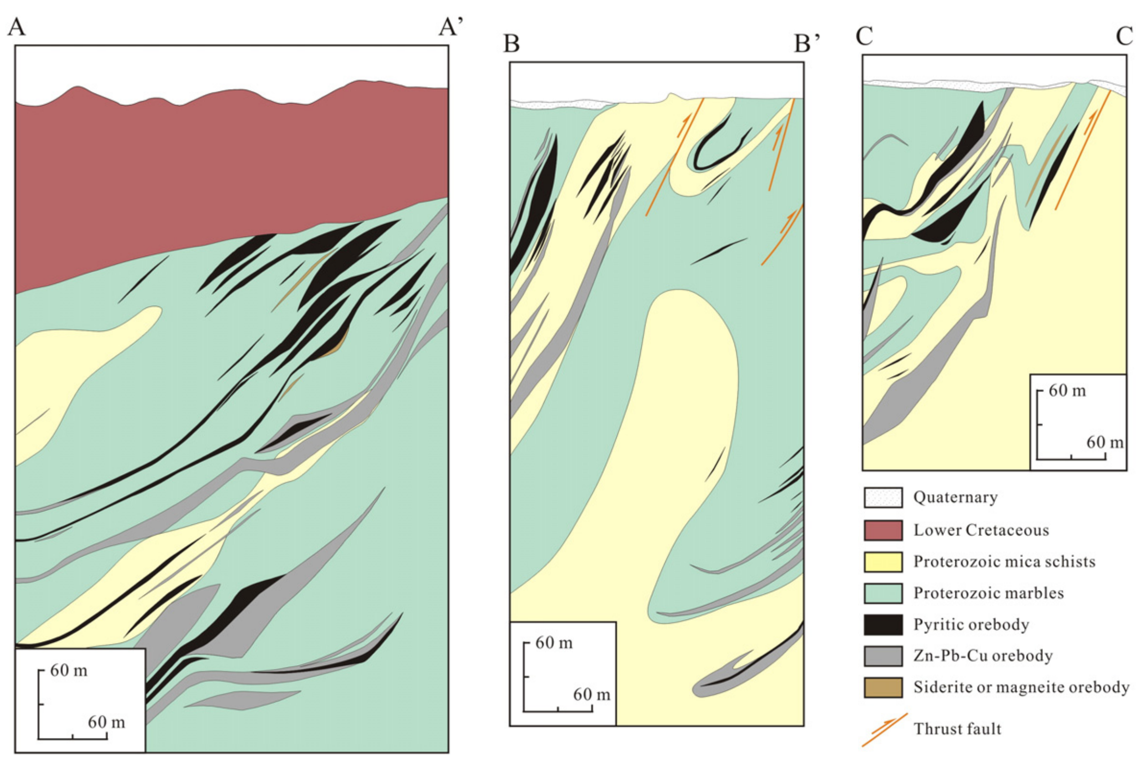

Fig. 4. Cross section of orebodies of the Dongshengmiao deposit (modified after Wulatehouqi Zijin Mining Group Co. Ltd, 2008).

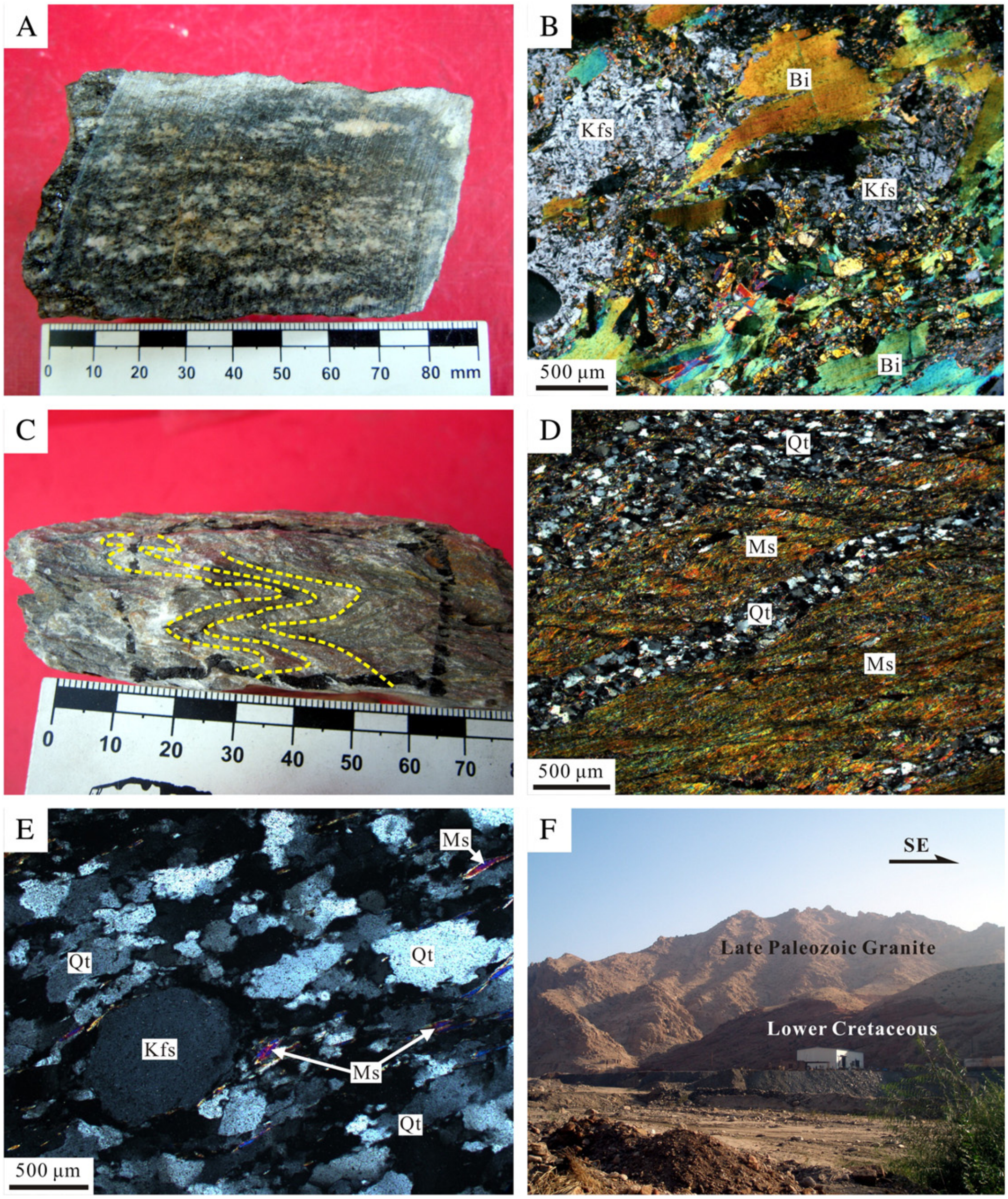

Fig. 5. Host rocks of the Dongshengmiao ore deposit. Abbreviations: Bi = biotite; Pl = plagioclase; Ms = muscovite; Qt = quartz; Kfs = K-feldspar. (A) Archean gneiss (DSM028; hand specimen). (B) Archean gneiss (same sample as A; crossed polars). (C) Proterozoic muscovite schist. Asymmetrical folds indicate shear deformation (DSM021; hand specimen). (D) Proterozoic muscovite schist (same sample as C; crossed polars). (E) Mylonitized Proterozoic K-feldspar-bearing quartzite. Quartz shows plastic deformation, whereas K-feldspar is resistant from plastic deformation (crossed polars). (F) Exposure showing a northwest-dipping thrust fault placing Late Paleozoic granite over Lower Cretaceous red sandstone, conglomerate and mudstone.

rocks and are separated from Late Paleozoic granites by a thrust fault along their northwest margin (Figs. 3, 5F). The Lower Cretaceous sediments have been interpreted as being deposited in a foreland basin formed during crustal shortening (Darby and Ritts, 2007). Conglomerate clasts are mainly composed of granite and quartzite (Wulatehouqi Zijin Mining Group Co. Ltd, 2008), indicating a granite source to the northwest (Fig. 2). They were deposited as the granite was being uplifted and eroded due to movement on the northwest-dipping thrust fault. This is consistent with the conclusion of Darby and Ritts (2007) that the lower Cretaceous sediments were deposited during northwest-southeast crustal shortening.

Several northeast-trending thrust faults occur in the mining area (Fig. 3). These thrust faults are generally developed parallel to sedimentary bedding (Suo, 1992), and consistently dip northwest at 30–45° (Hu et al., 1981), similar to the orebodies. Minimum displacements on the major thrusts in the mining area are 300 m (Hu et al., 1981). Mylonites are well developed adjacent to the thrust faults (Fig. 5E; Suo, 1992), whereas rocks away from thrust faults are weakly sheared and asymmetrically folded (Fig. 5C, D). Yang (1998) has pointed out that mylonites in the Dongshengmiao mining area are part of a regional northeast-trending shear zone, which extends over tens of kilometers, is 1–2 km wide, and is related to the thrust faults. In a mylonitized K-feldspar-bearing quartzite, quartz shows ductile deformation, whereas K-feldspar is free from ductile deformation (Fig. 5E). This suggests that mylonitization was characterized by brittle–ductile deformation, consistent with the P–T regime of lower greenschist facies regional metamorphism, and consequently indicates a synmetamorphic shear deformation.

Dongshengmiao is a giant Zn–Pb–Cu deposit with reserves of 4.83 Mt Zn at an average grade of 2.85% Zn, 0.96 Mt Pb at 0.67% Pb, and 0.11 Mt Cu at 0.86% Cu (Long, 2009). Besides, massive pyrite is also mined for the purpose of making sulfuric acid. Orebodies are hosted in lower greenschist facies Proterozoic rocks and overlain by Lower Cretaceous sediments (Fig. 4) that are not shown in Fig. 3. Orebodies are generally stratiform and stratabound, but locally cut across different lithological units of the host rocks (Fig. 4). They are mostly northeast-trending and northwest-dipping, with dips of 25°–65° (Fig. 4; Wulatehouqi Zijin Mining Group Co. Ltd, 2008), and show evidence of asymmetric folding (Fig. 4).

4. Petrologic characteristics of ores

A total of 103 samples of ores and host rocks were collected and 118 thin sections were prepared for petrographic study, which was carried out using conventional optical and scanning electron microscopy. A FEI-QUANTA650FEG scanning electron microscopic (SEM) at Peking University was used to obtain backscatter electron images and compositions (EDS spectrometer) of carbonates. The chemical composition of sphalerite was obtained using a JEOL JXA-8100 electron microprobe in Peking University. Operating conditions of the electron microprobe were 20 kV accelerating voltage, 10 nA beam current with 10 s measurement time and 1 μm spot size. Natural and synthetic minerals by the American SPI were used as standards. The ZAF method was used for data reduction of sulfides.

4.1. Massive pyrite

Massive pyrite is very common in the Dongshengmiao deposit (Fig. 6A–D), and is mined for sulfuric acids. Although most massive pyrite is strongly recrystallized, fine-grained pyrite is still locally preserved (Fig. 6A, B). The massive fine-grained massive pyrite ores were tectonically brecciated, and cemented by coarse-grained sulfides (chalcopyrite, pyrrhotite, sphalerite, and pyrite) and hydrothermal gangue minerals (biotite, quartz, and carbonate) (Fig. 6A, B), indicating their pre-tectonic origin.

The fine-grained pyrite was locally recrystallized (Fig. 6C), especially at contact with coarse-grained hydrothermal sulfides (e.g., chalcopyrite; Fig. 6B), suggesting a fluid-assisted recrystallization. Due to regional metamorphism and pervasive fluid activity, most massive pyrite ores were totally recrystallized, showing triple-junction texture (Fig. 6D). Recrystallized pyrite crystals are often flattened and display preferential orientation (Fig. 6D), indicating that the recrystallization process took place under compressional stress, i.e., regional metamorphism.

4.2. Zn–Pb–Cu mineralization

In a strongly mylonitized host rock, which is composed of oriented fine-grained ankerite and biotite, penetrative sulfide-bearing veinlets occur parallel to the mylonite foliation (Fig. 7A, B), together with hydrothermal gangue minerals such as coarse-grained quartz, ankerite and biotite (Fig. 7B). Parallel to the mylonite foliations and the hydrothermal veinlets, rhombic spaces were formed by shearing, and are filled with sulfides and hydrothermal gangue minerals (Fig. 7C). In the same sample, numerous fine-grained pyrite grains are disseminated in the host ankerite. SEM observation revealed that the pyrite grains are distributed along microfractures parallel to shear bands and accompanying hydrothermal minerals such as apatite (Fig. 7D). Compared with mineral elongation in the host rock, hydrothermal quartz and ankerite are essentially unstrained (Fig. 7B, C), although a weak deformation is indicated by the undulose extinction in quartz (Fig. 7C).

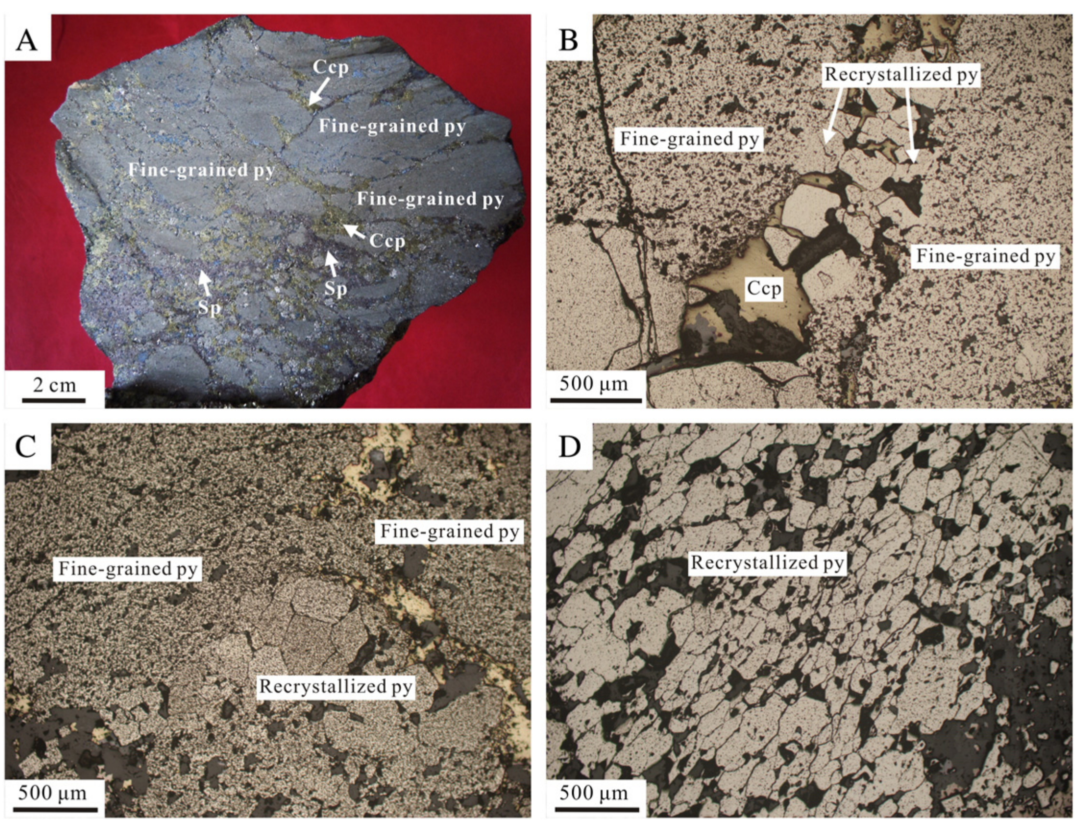

Fig. 6. Petrological characteristics massive pyrite. Abbreviations: Py = pyrite; Ccp = chalcopyrite. (A) Cataclastically deformed fine-grained pyrite cemented by hydrothermal sulfides (hand specimen). (B) Clasts of fine-grained pyrite cemented by hydrothermal chalcopyrite. Fine-grained pyrite recrystallized at contact with hydrothermal chalcopyrite (reflected light). (C) Partly recrystallized fine-grained pyrite, showing triple-junction texture (reflected light). (D) Totally recrystallized massive pyrite ore. Pyrite crystals are flattened and display preferential orientation, indicating that recrystallization process occurred under compressional stress (reflected light).

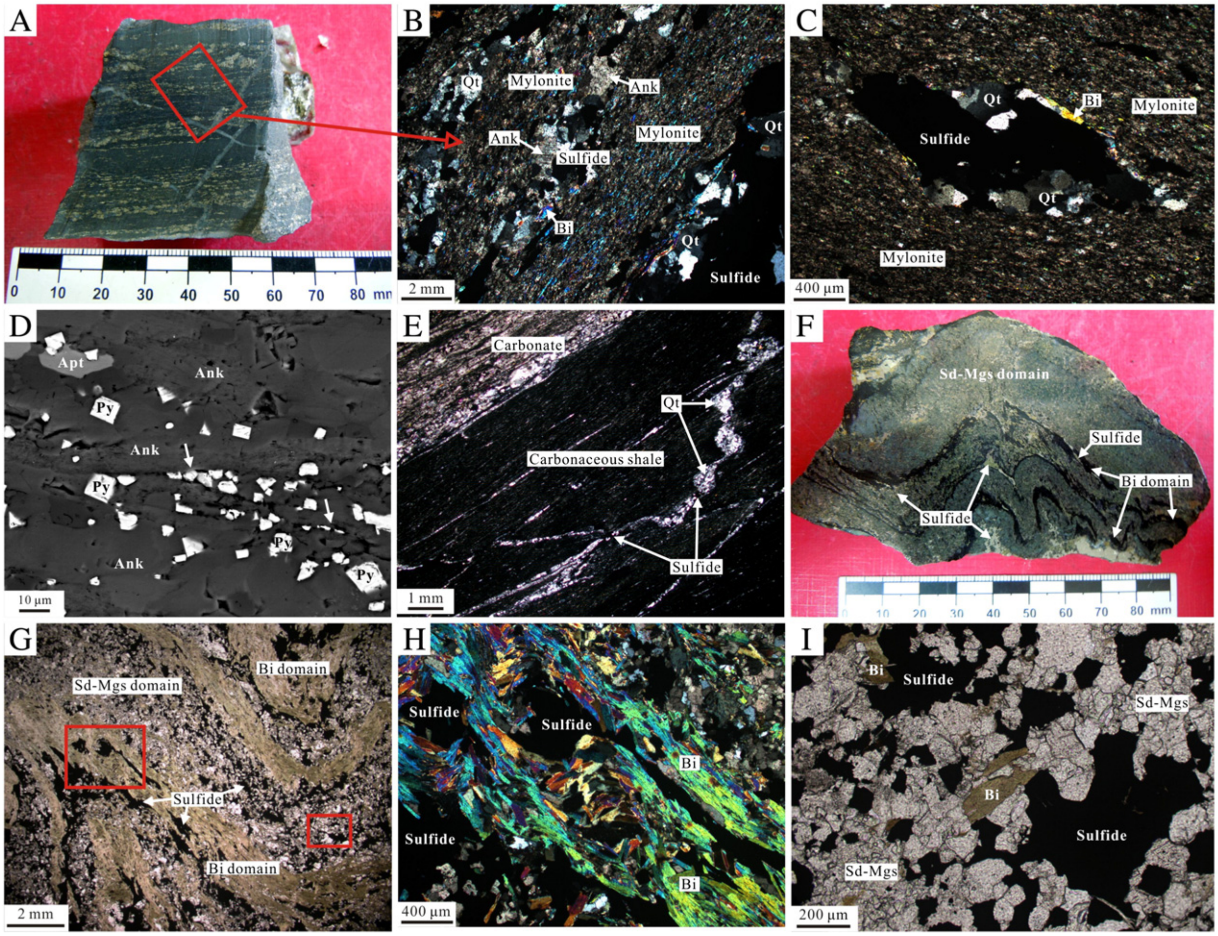

Fig. 7. Characteristics of the Zn–Pb–Cu ores, part one. Abbreviations: Ank = ankerite; Apt = apatite; Sd–Mgs = siderite–magnesite. Other abbreviations are as in Figs. 5 and 6. (A) Penetrative syntectonic veinlets developed parallel to mylonite foliations of the host rock (hand specimen). (B) Hydrothermal veinlets composed of sulfides, quartz, ankerite and biotite developed parallel to mylonite foliation of the host rock (magnification of box area in A, crossed polars). (C) Rhombic sulfide-filled space developed parallel to the mylonite foliation. Sulfides were precipitated with hydrothermal quartz and biotite and the hydrothermal minerals are generally unstrained (same sample as A, B; crossed polars). (D) Fine-grained pyrite precipitated along microfractures of ankerite (arrows, same sample as A–C; SEM image). (E) Carbonaceous shale-hosted ore. Sulfide-bearing quartz has been progressively deformed by shearing (plane-polarized light). (F) In an asymmetrically folded rock, sulfides were precipitated in hinge regions and axial-plane cleavages of the asymmetrical fold (polished section). (G) In a rock composed of interlayered biotite and siderite–magnesite, sulfides precipitated parallel to the foliation in biotite and along grain boundaries in siderite–magnesite (same sample as F; plane-polarized light). (H) Sulfides precipitated in the extensional space formed during asymmetrical folding of the host rock (magnification of the left box area in G, crossed polars). (I) Sulfides and hydrothermal biotite precipitated along grain boundaries of siderite–magnesite (magnification of the right box area in G, plane-polarized light).

In a host rock composed of interlayered carbonaceous shale and carbonates, host rock minerals are strongly elongated and oriented, forming shear bands (Fig. 7E). Sulfide-bearing quartz veinlets are developed generally parallel to shear bands, and have been progressively and plastically deformed by shearing (Fig. 7E). The geometry of the deformed veinlets indicates that they were deformed under similar shear stress as that responsible for host rock mylonitization (Fig. 7E).

In addition to mylonite, asymmetrical folding is also formed as a result of shear deformation (Passchier and Trouw, 2005). In an asymmetrically folded host rock that composed of interlayered biotite and siderite–magnesite (Fig. 7F, G), mineralization styles vary in different parts of the host rock. In biotite-rich domains, sulfides (and magnetite) tended to occur at hinge regions and axial-plane cleavages of the asymmetrical folds (Fig. 7F, G), or as filling in extensional spaces that formed during asymmetrical folding (Fig. 7H). In siderite–magnesite domains, sulfides occur together with hydrothermal biotite along grain boundaries of siderite–magnesite, and locally replace host siderite–magnesite (Fig. 7I). Similar replacement textures are commonly observed in high-grade Zn–Pb ores, which are also characterized by sulfides replacing ore-hosting siderite–magnesite along grain boundaries (Fig. 8A). Hydrothermal biotite commonly accompanies sulfides (Fig. 7I), especially at contacts between sulfides and siderite–magnesite (Fig. 8A). Siderite–magnesite of the host rock (molar Fe/(Fe + Mg) = 0.54) was hydrothermally altered along grain boundaries to more magnesian compositions (molar Fe/(Fe + Mg) = 0.45; Fig. 8B). Among the ore minerals, chalcopyrite has been corroded by magnetite with embayed boundaries (Fig. 8C).

Breccia Pb–Zn ore is composed of fragments of foliated host rocks (mica schist, siderite–magnesite; Fig. 8D, E), and cemented by sulfides (sphalerite, pyrite, pyrrhotite and galena) and hydrothermal gangue minerals (quartz, siderite–magnesite, biotite; Fig. 8E, F), indicating that sulfide formation postdates host rock foliation. Host rock cataclastic deformation (i.e., brecciation) and Pb–Zn mineralization took place simultaneously and under shear deformation, manifested by the rotated host rock fragments (Fig. 8D).

Vein-type ores, as a typical signature of hydrothermal mineralization, are observed in the Dongshengmiao deposit (Fig. 8G–I). Muscovite from a chalcopyrite-bearing quartz–K-feldspar–muscovite vein (sample DSM042; Fig. 8G–I) was selected for $^{39}Ar/^{40}Ar$ geochronological study, and its petrological characters are introduced below. Muscovite and sulfides (mainly pyrrhotite and chalcopyrite) are intimately associated and mostly occur along the vein–wall rock contact (Fig. 8G), indicating that

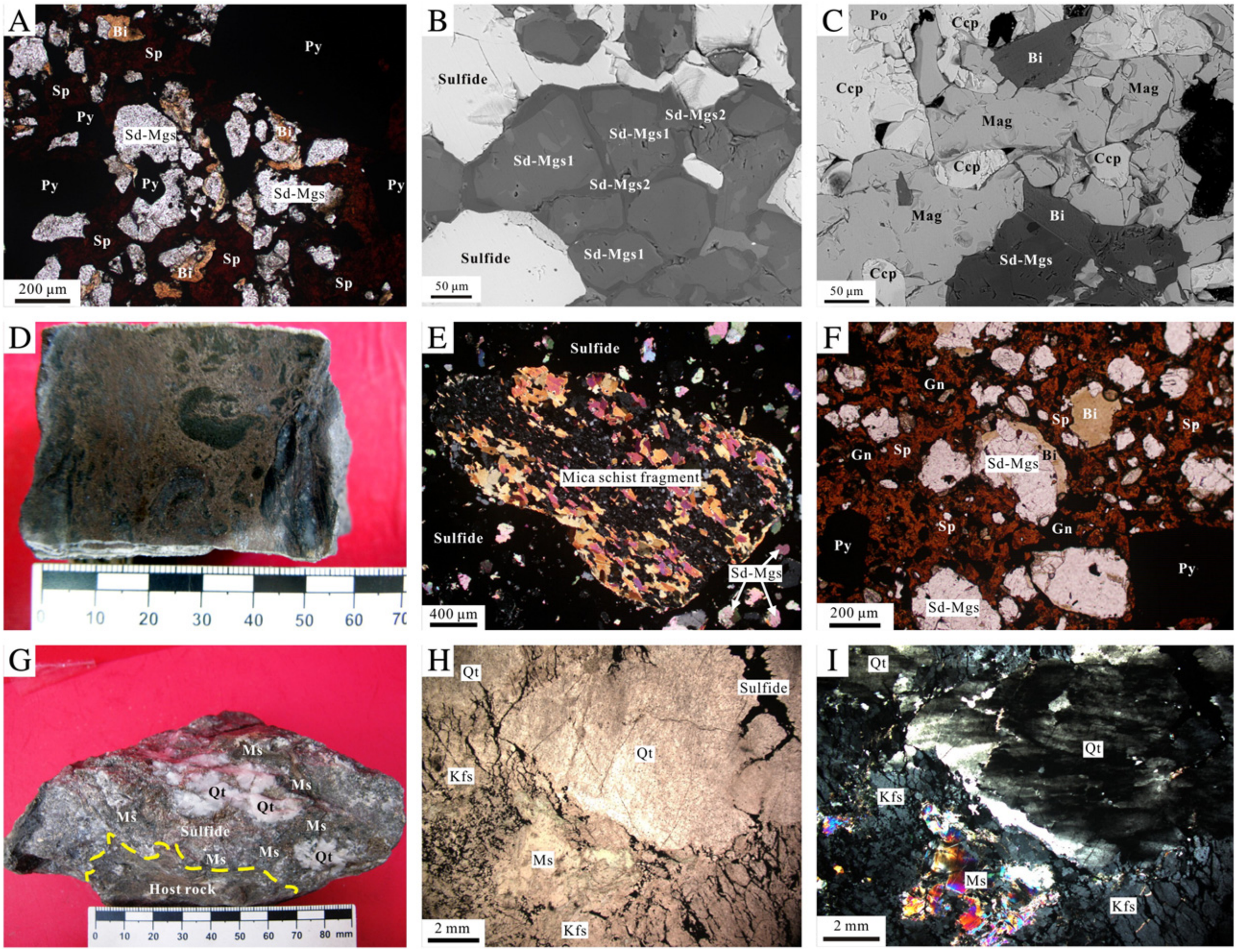

Fig. 8. Characteristics of Zn–Cu–Pb ores, part two. Abbreviations: Sp = sphalerite; Gn = galena. Other abbreviations are given in Figs. 5–7. (A) High-grade Pb–Zn ore. Sulfides along grain boundaries of siderite–magnesite and corroded siderite–magnesite. Biotite at contact between sulfides and host rock siderite–magnesite (plane-polarized light). (B) Fe-rich siderite–magnesite of host rock (Sd–Mag1) altered by ore-fluid along grain boundaries, forming more Mg-rich siderite–magnesite (Sd–Mag2). Sulfides are intimately associated with Mg-rich siderite–magnesite (backscatter electron image). (C) Chalcopyrite corroded by magnetite with embayed boundaries, indicating that both minerals were precipitated from fluids. Biotite at contact between magnetite and siderite–magnesite host rock (backscatter electron image). (D) Breccia ore. Breccia elements are rotated in the middle of the ore (hand specimen). (E) Fragment of ore-hosting mica schist in sulfide matrix (same sample as D; crossed polars). (F) Hydrothermal biotite at contact between siderite–magnesite fragment and matrix sulfide (same sample as D, E; plane-polarized light). (G) Vein-type ore. Muscovite and sulfides at the contact between vein and host rock (DSM042, hand specimen). (H) Vein-type ore. Oriented sulfide-filled microfractures in K-feldspar (same sample as G; plane-polarized light). (I) Same field of view as H, but in reflected light. Oriented subgrains are well-developed in hydrothermal quartz.

muscovite is coeval with hydrothermal mineralization. Compared with metamorphic muscovite in the host rock, hydrothermal muscovite in the vein-type ore has much greater grain size and contains sulfide inclusion. Oriented microfracutures were well developed within K-feldspar crystals (Fig. 8H), indicating that K-feldspar underwent brittle deformation during mineralization. In contrast, hydrothermal quartz shows evidence of progressive plastic deformation, with the development of subgrains (Fig. 8I). These quartz subgrains are oriented (Fig. 8I) and parallel to the vein–host rock contact.

4.3. Mineral chemistry of sphalerite

The FeS contents of sphalerite correlated with formation pressure, if sphalerite grew in equilibrium with pyrite and pyrrhotite (Hutchison and Scott, 1981). The chemical composition of the sphalerite that is in textural equilibrium with both pyrite and pyrrhotite was obtained using electron microprobe (Table 1), to reveal the pressure and crustal depth of Zn–Pb–Cu mineralization. Sphalerite in this deposit has FeS contents ranging from 16.3 to 17.9 at.% FeS, resulting in calculated formation pressures between 2.1 and 3.4 kbar, with an average of 2.9 ± 0.5 kbar (1σ; n = 15; Table 1). This corresponds to an ore-forming depth of ca. 7–10 km.

5. $^{39}Ar/^{40}Ar$ geochronology

5.1. Sampling and analysis methods

Three samples were selected for $^{39}Ar/^{40}Ar$ geochronology: (1) biotite from an Archean gneiss in the ore field (DSM028, Fig. 5A, B). This sample is composed mainly of K-feldspar, plagioclase, biotite and quartz (Fig. 5B), suggesting upper amphibolite facies conditions of metamorphism. (2) Muscovite from an ore-hosting Proterozoic muscovite schist (DSM021, Fig. 5C, D). This sample is composed of muscovite and quartz, and represents lower greenschist facies metamorphism (Fig. 5D). This sample has undergone shear deformation, as evidenced by asymmetric folding (Fig. 5C, D). Quartz and muscovite show evidence of plastic deformation, indicating that the temperature of shear deformation was higher than 300 °C (Passchier and Trouw, 2005), and consistent with conditions of lower greenschist facies metamorphism. (3) Hydrothermal muscovite from a sulfide-bearing quartz–K-feldspar–muscovite vein (DSM042, Fig. 8G–I). A detailed description on this sample is given in Section 4.2.

Muscovite and biotite were separated from the samples and crushed to 0.18–0.28 mm. About 2 mg muscovite or biotite was packed in pure aluminous foil for each sample. The foils were placed in evacuated

Table 1
Electron probe microanalysis of sphalerite in Cu ores in the Dongshengmiao deposit (wt.%).

Mineral	Fe	As	S	Ni	Pb	Cu	Ag	Zn	Cd	Au	Sb	Total	Geobarometer (kbar)
Sphalerite	10.46	0.02	31.26	<mdl	0.09	<mdl	<mdl	58.12	0.12	0.14	<mdl	100.2	2.48
Sphalerite	9.79	0.02	31.51	<mdl	0.11	0.04	<mdl	58.49	0.11	0.29	0.03	100.37	3.32
Sphalerite	10.75	0.01	31.68	<mdl	0.01	0.01	<mdl	57.89	0.15	0.23	<mdl	100.72	2.12
Sphalerite	10.1	0.01	32.34	<mdl	0.02	0.02	<mdl	56.76	0.08	<mdl	0.02	99.34	2.61
Sphalerite	10.49	0.03	32.06	0.01	0.14	<mdl	0.03	57.17	0.08	0.1	0.03	100.13	2.25
Sphalerite	9.62	<mdl	32.11	0.01	0.14	0.08	0.02	57.25	0.05	<mdl	<mdl	99.27	3.27
Sphalerite	9.69	<mdl	32.21	<mdl	0.1	<mdl	0.04	57.39	0.14	0.21	<mdl	99.78	3.21
Sphalerite	10.41	0.07	32.39	<mdl	0.11	0.06	<mdl	56.74	0.15	<mdl	0.01	99.93	2.25
Sphalerite	9.57	<mdl	32.13	<mdl	0.01	<mdl	<mdl	57.04	0.05	0.42	<mdl	99.22	3.29
Sphalerite	9.8	<mdl	31.91	<mdl	0.11	<mdl	<mdl	56.99	0.19	<mdl	<mdl	99	3.00
Sphalerite	9.54	<mdl	32.25	0.01	0.08	<mdl	<mdl	57.01	0.15	0.31	<mdl	99.36	3.32
Sphalerite	9.51	<mdl	32.29	<mdl	0.03	<mdl	0.03	57.22	0.15	0.49	<mdl	99.72	3.40
Sphalerite	9.85	<mdl	32.04	0.01	0.06	<mdl	<mdl	57.24	0.14	0.08	0.02	99.46	2.99
Sphalerite	9.62	0.04	31.98	0.02	0.09	0.03	0.02	57.17	0.1	0.17	0.01	99.26	3.25
Sphalerite	9.67	0.11	32.65	<mdl	0.07	<mdl	<mdl	56.85	0.11	0.03	<mdl	99.48	3.13

Minimum detection limits are 0.01 wt.% for all elements, mdl = minimum detection limit.

quartz tubes and irradiated in the 49-2 Nuclear Reactor at the Institute of Chinese Atomic Energy for 24 h, with an irradiation flux of 2.2464×10^{18} fast neutrons/cm^2. Neutron flux variation (J) was measured using the standard mineral Zhoukoudian biotite (ZBH-25; 132.7 Ma). After irradiation, the samples were heated to total fusion in a tantalum furnace, during 10–14 stepwise-heating stages. Extracted gas was analyzed using a RGA10 mass spectrometer at the Key Laboratory of Orogenic Belts and Crustal Evolution, Peking University. Argon isotope data were corrected for system blanks, mass discrimination, and interfering neutron reactions with Ca and K and are listed in Table 2 (as supplementary data). Correction factors are: $(^{36}Ar/^{37}Ar)_{Ca} = 0.000271$, $(^{39}Ar/^{37}Ar)_{Ca} = 0.000652$, and $(^{40}Ar/^{39}Ar)_K = 0.00703$. The analyzed argon isotope data were corrected using the $^{40}Ar/^{39}Ar$ Dating 1.2 software developed by the Key Laboratory of Orogenic Belts and Crustal Evolution, Peking University. Plateau and isochron ages were calculated using the Isoplot 3.0 software of Ludwig (2003).

5.2. Results and interpretation

5.2.1. Biotite in the Archean gneiss (DSM028)

Biotite in the Archean gneiss DSM028 yields a plateau age of 123.1 ± 0.9 Ma, corresponding to six stages and 87.7% ^{39}Ar release, with a MSWD of 0.53 (Fig. 9A). The six data points define an isochron age of 123.0 ± 1.9 Ma, with a MSWD of 6.2 and an initial $^{40}Ar/^{36}Ar$ of 297 ± 47 (Fig. 9A). The consistence between the plateau and isochron ages and approximation of the initial $^{40}Ar/^{36}Ar$ to that of the atmosphere (295.5 ± 5) suggest that the age is reliable. This sample underwent upper amphibolites facies metamorphism, therefore the age of ca. 123 Ma is the time when the rock was uplifted and cooled below the closure temperature for biotite (ca. 300 °C, Chiaradia et al., 2013).

5.2.2. Muscovite in the ore-hosting schist (DSM021)

Muscovite in the ore-hosting Proterozoic muscovite schist DSM021 yields a plateau age of 135.5 ± 0.9 Ma, corresponding to six stages and 82.2% ^{39}Ar release, with a MSWD of 0.114 (Fig. 9B). An isochron age of 135.7 ± 1.4 Ma is given by the six data points, with a MSWD of 1.17 and an initial $^{40}Ar/^{36}Ar$ of 290 ± 7 (Fig. 9B). The isochron age is close to the plateau age, and the initial $^{40}Ar/^{36}Ar$ is close to that of the atmosphere, indicating that the age is reliable. As mentioned above, this sample has been metamorphosed to lower greenschist facies conditions (ca. 350–500 °C; Miyashiro, 1994), and underwent shear deformation at temperatures higher than 300 °C. These temperatures are close to the closure temperature of muscovite (ca. 350 °C; Chiaradia et al., 2013); therefore the age of ca. 136 Ma is interpreted as that of peak metamorphism and shear deformation of the ore-hosting muscovite schist.

5.2.3. Hydrothermal muscovite (DSM042)

Muscovite from a chalcopyrite-bearing quartz–K-feldspar–muscovite vein (DSM042) yields a plateau age of 135.6 ± 0.8 Ma, corresponding to eight stages and 90.7% ^{39}Ar release, with a MSWD of 0.46 (Fig. 9C). The corresponding isochron age given by the eight data points is 135.4 ± 0.9 Ma, with a MSWD of 1.4 and an initial $^{40}Ar/^{36}Ar$ of 309 ± 24 (Fig. 9C). The reliability of the age is indicated by the consistence between the plateau and isochron ages and the initial $^{40}Ar/^{36}Ar$ that is close to that of the atmosphere. Petrological characteristics of Zn–Pb–Cu ores indicate that they were precipitated from an epigenetic hydrothermal solution, and the sulfide-bearing quartz–K-feldspar–muscovite vein (DSM042) represents a depositional site with high fluid flux (see the discussions in Section 6.2). Muscovite in this sample is coeval with Zn–Pb–Cu mineralization, manifested by its intimate spatial relationship with Cu-sulfides and sulfide inclusions within it. The flat age spectrum (Fig. 9C) indicates that this sample has not been thermally disturbed (i.e., reheated) after its crystallization (McDougall and Harrison, 1999). This is consistent with the observation that hydrothermal sulfides and syn-ore gangue minerals (e.g., quartz and carbonates) are generally free from recrystallization. The lower greenschist facies hydrothermal gangue mineral assemblage and the brittle–ductile ore-forming structures in Zn–Pb–Cu ores (see discussions in Section 6.2) indicate that Zn–Pb–Cu mineralization temperature was close to the closure temperature for muscovite (ca. 350 °C). Therefore the muscovite age of ca. 136 Ma is interpreted as the time of Zn–Pb–Cu sulfide precipitation.

6. Discussion

6.1. Evidence of syngenetic mineralization

Although most massive pyrite ores are totally recrystallized with reworking by hydrothermal fluids (Fig. 6D), the fine-grained pyrite is a typical index of syngenetic sulfide (Fig. 6A–C; Leach et al., 2005). In addition to pre-tectonic fine-grained massive pyrite (Fig. 6A–C) and abundant recrystallized massive pyrite ores (Fig. 6D), the syngenetic mineralization event is also manifested by the presence of marcasite in S-rich ores and fine-grained tourmaline in the footwall of S-rich orebodies (Zhang et al., 2010b). Siderite layers and B, Mn, P, Ba enriched layers are present in the mining field (Zhai et al., 2008; Zhang et al., 2010b), which are characteristic of syngenetic ore-forming systems (e.g., Leach et al., 2005). Submarine volcanic activity manifested by the presence of bimodal volcanic rocks also provides a favorable geological

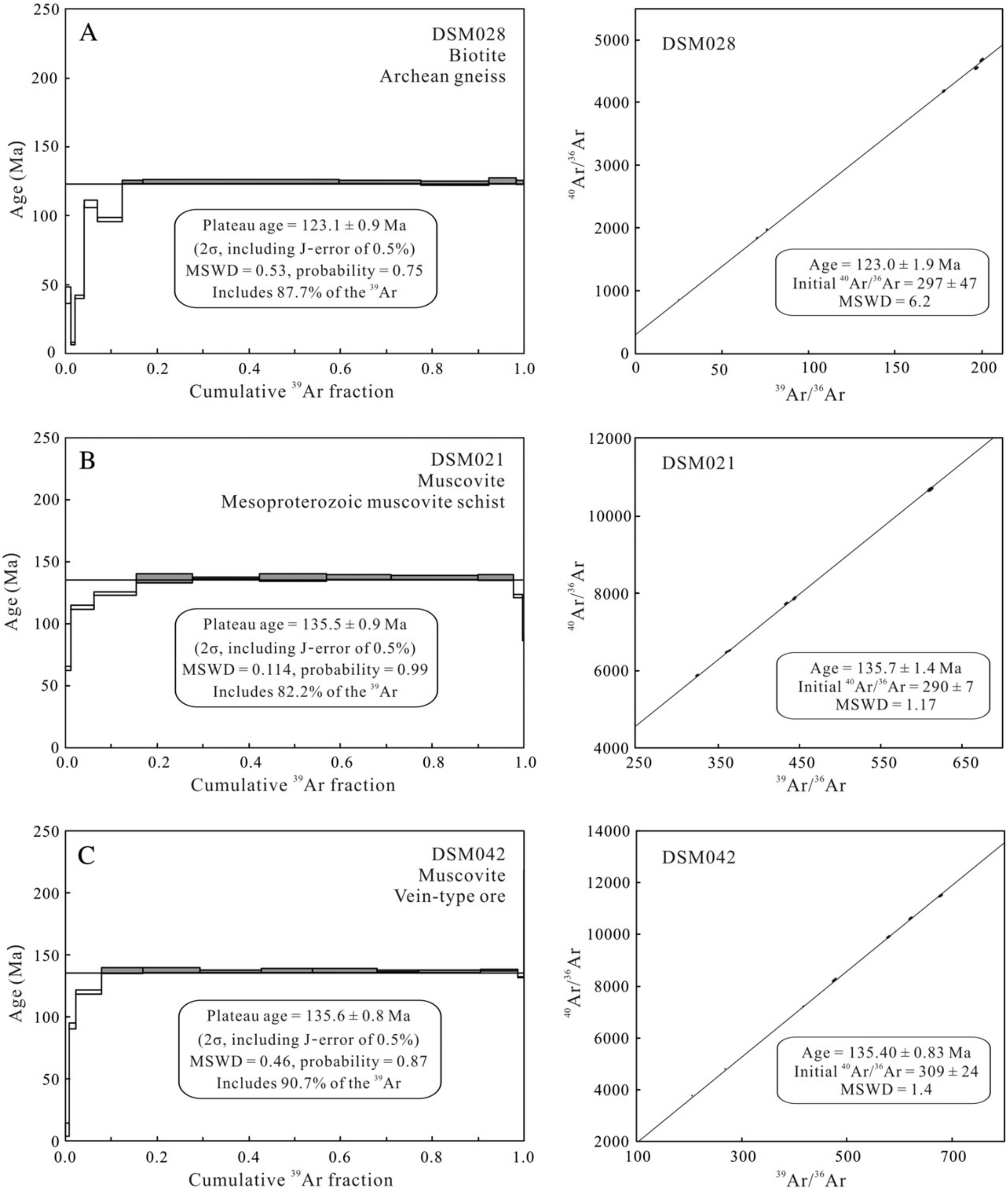

Fig. 9. $^{40}Ar/^{39}Ar$ age spectra and isochron plots.

setting for development of submarine hydrothermal systems during rifting (Peng and Zhai, 1997).

Most importantly, the compilation of lead isotope data of sulfides (Huang, 2009; Li et al., 1986) indicates that sulfides of the Dongshengmiao are poor in radiogenic lead, and yield two-stage model ages of ~2000 to ~1750 Ma, consistent with the depositional age of ore-hosting rift rocks (Fig. 10). This indicates that the ore-forming metals were originally sourced from stratabound sulfides during Proterozoic times. Although no syngenetic Zn–Pb–Cu ores have been found in this study, the sulfides poor in radiogenic lead were unlikely generated from a source with normal crustal Pb abundance in Mesozoic time (Leach et al., 1998), i.e., a syngenetic pre-enrichment was involved in ore-forming process.

6.2. Syntectonic and synmetamorphic Zn–Pb–Cu remobilization

Unlike massive pyrite, Zn–Pb–Cu ores show abundant signatures typical of epigenetic hydrothermal mineralization. As introduced above, sulfides were originally deposited as stratabound deposit within the Proterozoic rift sequence. However, as a result of significant fluid-assisted metal remobilization, the present form of all Zn–Pb–Cu ores

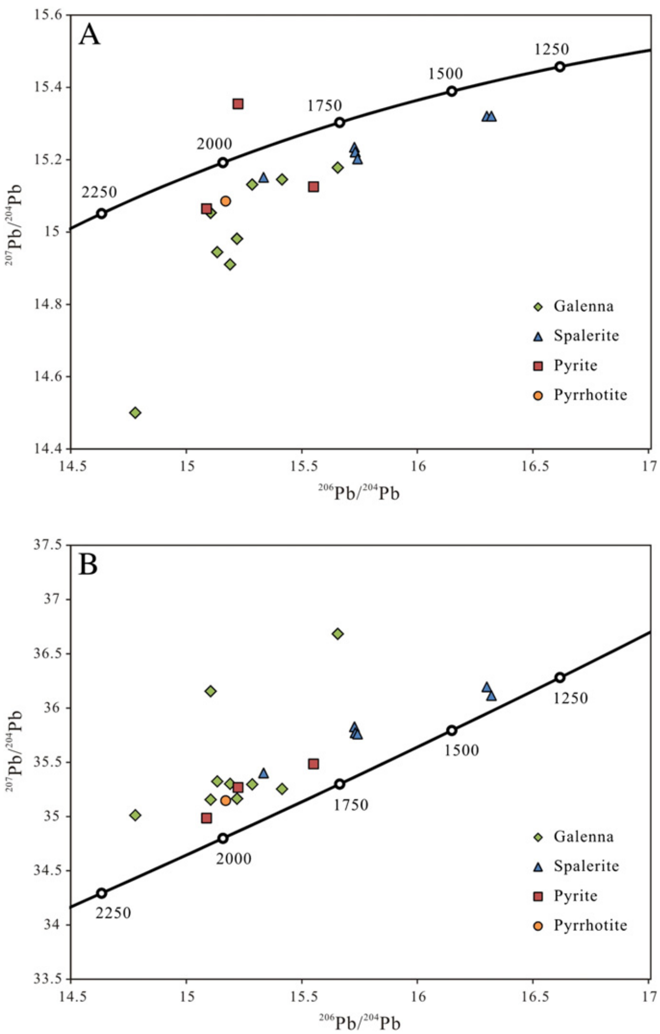

Fig. 10. Lead isotope data on sulfides. The two-stage lead growth curve is from Stacey and Kramers (1975) and shown as the bold curve. The numbers along the growth curve are dates in the past, in millions of years, representing the time when lead was drawn from its source. The lead isotope data of sulfides are compiled from Huang (2009) and Li et al. (1986). (A) $^{206}Pb/^{204}Pb$–$^{207}Pb/^{204}Pb$ diagram. (B) $^{206}Pb/^{204}Pb$–$^{208}Pb/^{204}Pb$ diagram.

that were observed in this study show signatures of epigenetic hydrothermal mineralization.

During the remobilization, Zn–Pb–Cu ores in the Dongshengmiao deposit were precipitated from hydrothermal solutions, manifested by the intimate association between sulfides and hydrothermal gangue minerals, such as quartz, carbonates and biotite (Figs. 7B–E, I, 8A–C, F). The presence of sulfide-bearing veinlets (Fig. 7A, B, E), vein-type mineralization (Fig. 8G–I), and the texture of chalcopyrite corrosion by magnetite (Fig. 8C) is also characteristics of hydrothermal mineralization (Gu et al., 2004).

The Zn–Pb–Cu mineralization type varies at different depositional sites, as a result of varying fluid fluxes. The vein-type mineralization (Fig. 8G–I) is an indicator of channelized ore-fluid with high flux. On the contrary, the syntectonic veinlets (Fig. 7A, B) and sulfide-filling microfractures (Fig. 7D) are results of pervasive ore-fluids with low fluid flux. Sulfide precipitation (Figs. 7I, 8A) and hydrothermal alteration (Fig. 8B) along grain boundaries of siderite–magnesite of host rocks also indicate a pervasive flow by ore-fluids infiltrating the host rock.

Hydrothermal gangue minerals associated with Zn–Pb–Cu sulfides include biotite, chlorite, muscovite, quartz and carbonates (Figs. 7B, C, E, I, 8A, C, F), which are similar to the metamorphic mineral assemblage of the greenschist facies host rocks, suggesting that regional metamorphism and the Zn–Pb–Cu remobilization occurred at about the same temperature, i.e., synmetamorphic remobilization. In both metamorphic host rock and hydrothermal veinlets, the color of biotite (an indication of its formation temperature; Miyashiro, 1994) is consistently brown regardless of its origin (Figs. 7G, I, 8A), also indicating the synmetamorphic fluid-assisted remobilization.

The contrasting deformation styles of quartz (ductile deformation; Fig. 8I) and K-feldspar (brittle deformation; Fig. 8H) in vein-type ores indicate a brittle–ductile regime during remobilization (Passchier and Trouw, 2005), which is characteristic of greenschist facies conditions (Goldfarb et al., 2005). Based on the sphalerite geobarometer, Zn–Pb–Cu remobilization took place at ~7–10 km, consistent with the crustal depth of brittle–ductile regime and greenschist facies condition. All these observations indicate that Zn–Pb–Cu remobilization was coeval with greenschist metamorphism of the host rocks, i.e., a synmetamorphic Zn–Pb–Cu remobilization.

During sulfide precipitation, ore-fluids interacted with the ore-hosting siderite–magnesite in a skarn-like environment, shown by the presence of hydrothermal biotite accompanying sulfides (Fig. 7I), especially at contacts between sulfides and siderite–magnesite (Fig. 8A). The compositions of carbonates were investigated in seven samples using energy dispersive spectrometer in a SEM. High-grade massive and disseminated ores (five samples) are hosted in siderite–magnesite ($(Fe, Mg)CO_3$, molar Fe/(Fe + Mg) = 0.48–0.65); within a low-grade sheeted veinlet (one sample), ore is hosted in ankerite ($Ca(Fe, Mg)(CO_3)_2$, molar Fe/(Fe + Mg + Ca) = 0.10); and a barren host rock (one sample) is composed of Fe-poor dolomite ($CaMg(CO_3)_2$). This indicates that chemically active Fe-rich carbonates are ideal sinks for sulfide redistribution via a skarn-like fluid–rock interaction. Similarly, the observation that Fe-rich host rocks are ideal for mineralization has been reported in orogenic gold and shear zone controlled epigenetic Cu deposits (e.g., Goldfarb et al., 2005; Gu et al., 2004, 2005, 2007; Zhong et al., 2012).

Sulfides and hydrothermal gangue minerals were precipitated parallel to the mylonitic foliation (Fig. 7A, B), indicating that ore-filling structures were developed during mylonitization of the host rock. Asymmetrical folding is another signature of shear deformation (Hatcher, 1995). Sulfides filling hinge regions, axial-plane cleavages, and extensional spaces of asymmetrical folds (Fig. 7F–H) imply that sulfide precipitation was coeval with shear deformation of the host rock. Rotated host rock fragments that were cemented by Zn–Pb-sulfides in breccia ores (Fig. 8D) indicate a shear stress during Zn–Pb–Cu remobilization. Fine-grained massive pyrite was tectonically brecciated and cemented by coarse grained Zn–Pb–Cu sulfides and hydrothermal gangue minerals (Fig. 6A), also indicating that fluid-assisted Zn–Pb–Cu remobilization was synchronous tectonic brecciation of syngenetic massive pyrite. The presence of progressively shear deformed sulfide-bearing veinlets (Fig. 7E) and undulating extinction of hydrothermal quartz (Figs. 7C, 8I) is typical indicators of syntectonic mineralization (Goldfarb et al., 2005). Compared with strongly deformed metamorphic minerals in the host mylonite, hydrothermal minerals were weakly deformed, indicating that Zn–Pb–Cu remobilization occurred late during the shearing event.

The age of regional metamorphism and shear deformation (135.5 ± 0.9 Ma, plateau age) is the same as the age of Zn–Pb–Cu remobilization (135.6 ± 0.8 Ma, plateau age). This is consistent with the synmetamorphic and syntectonic features of the Zn–Pb–Cu remobilization.

On the basis of our observation, it is highly probable that some stratabound syngenetic Zn–Pb–Cu orebodies are well preserved in this deposit, although all the observed Zn–Pb–Cu ores in this study show signatures of syntectonic hydrothermal mineralization. Nevertheless, a high degree of Zn–Pb–Cu remobilization via solution transfer can be confirmed by this study. The parental stratabound sulfides have been almost totally redistributed during regional metamorphism and deformation. The present form of Zn–Pb–Cu mineralization is largely controlled by the shear zone and chemically activity host rocks (e.g., Fe-rich carbonate), and shares many geological and geochemical similarities with orogenic gold deposits (Goldfarb et al., 2005). This is critical in understanding ore-controlling factors and targets of mineral exploration of this deposit, especially when establishing the mine field-scale model for mineral exploration.

6.3. Tectonic background of Early Cretaceous Zn–Pb–Cu remobilization

The 136 Ma regional metamorphism, deformation, and accompanying Zn–Pb–Cu remobilization are coeval with the Late Jurassic–Early Cretaceous intraplate orogenic belt in the Langshan district (Darby and Ritts, 2007; Gao, 2010) and adjacent areas (Darby and Ritts, 2002; Davis and Darby, 2010; Davis et al., 1998; Qi et al., 2007; Wang et al., 2004; Zhang et al., 2009a; Zheng et al., 1998).

In the Langshan district, this intraplate deformation event was characterized by strong compression followed by weak extension (Darby and Ritts, 2007). Two ages of the intraplate contraction event have been reported as 116 ± 1.8 Ma and 126 ± 1.1 Ma (biotite $^{39}Ar/^{40}Ar$, plateau ages), from mylonites of two shear zones in the Langshan district (Gao, 2010). This suggests that Zn–Pb–Cu remobilization of the Dongshengmiao deposit (ca. 136 Ma) occurred prior to the cessation of crustal shortening, and consequently during regional compression and related thrust faulting. The orebodies were asymmetrically folded (Fig. 4) and share similar occurrences with northwest-dipping thrust faults in the mining area (Figs. 3, 4). The geometry of the asymmetrically folded orebodies indicates that the remobilization was controlled by these northwest-dipping thrust faults and suffered progressive deformation (Fig. 4), i.e., syntectonic Zn–Pb–Cu remobilization. The orebodies are overlain by Early Cretaceous foreland basin sediments that formed during crustal shortening (Fig. 4), further suggesting that Zn–Pb–Cu remobilization occurred during regional contraction.

The orebodies, ore-hosting Proterozoic muscovite schist, and the Archean gneiss were exposed to the surface prior to deposition of the Lower Cretaceous sediments (Figs. 3, 4). The $^{40}Ar/^{39}Ar$ ages of muscovite from the Proterozoic host rocks and orebodies (ca. 136 Ma) and biotite from the Archean gneiss (123 Ma) represent the times when these rocks were at crustal depths with temperatures equal to their closure temperatures (ca. 350 and 300 °C respectively). The precise age of the Lower Cretaceous rocks is unknown, but they should be >100 Ma, the boundary between the Early and Late Cretaceous. These ages imply rapid uplift and exhumation during and after Zn–Pb–Cu remobilization in this area, and are also consistent with the fact that Zn–Pb–Cu remobilization was coeval regional contraction.

6.4. The multistage genetic model of the Dongshengmiao deposit

In the Proterozoic, a rift developed in the Langshan district. During deposition in the rift, submarine hydrothermal activity took place and resulted in stratabound Zn–Pb–Cu mineralization. Massive pyrite, siderite layers, and B, Mn, P and Ba enriched layers were also formed in the mining field accompanying Zn–Pb–Cu mineralization.

During the development of an intraplate orogenic belt in the Langshan and adjacent districts in the Early Cretaceous (ca. 136 Ma), most of the syngenetic Zn–Pb–Cu sulfides were remobilized and redistributed during regional metamorphism. Zn, Pb and Cu were transported in hydrothermal solutions, and the present form of the deposit is controlled by this large-scale remobilization process.

Accompanying regional metamorphism, synchronous thrust faults controlled redistribution of Zn–Pb–Cu orebodies. Some sulfides were precipitated from the channelized flow and formed the sheared vein-type ores, whereas most sulfides were precipitated along grain boundaries, microfractures, or mylonite foliations of the host rocks (i.e., pervasive flow). Chemically active lithological units, such as Fe-rich carbonates, provided favorable sites for Zn–Pb–Cu redistribution and the formation of high-grade ores. Most Zn–Pb–Cu-sulfides were redistributed at the depth of the brittle–ductile transition (ca. 7–10 km), but the occurrence of breccia Pb–Zn ores (Fig. 8D–F) suggests that some Pb–Zn-sulfides were precipitated at a shallower depth (i.e., brittle regime) during exhumation.

The ages of magmatic activity (Late Paleozoic) and migmatisation (2480 Ma) in the Dongshengmiao mining area are much older than the Zn–Pb–Cu remobilization (136 Ma). Therefore, contemporaneous metamorphic devolatilization (136 Ma) of the ore-hosting Proterozoic rift sequence is the most likely source of fluids for the Zn–Pb–Cu remobilization. A metamorphic origin of the fluid is supported by isotopic and fluid inclusion studies. Oxygen and hydrogen isotope ratios were obtained by analyzing hydrothermal quartz and mica, respectively (Ding et al., 1992). $\delta^{18}O$ and δD values of the ore-fluid were calculated at an estimated temperature of 350 °C, and they range from 11.0 to 14.7‰ and from −76 to −54‰, respectively (Ding et al., 1992). These values are consistent with isotope ratios of metamorphic fluids (Goldfarb et al., 1991). A fluid inclusion study indicates that the ore-fluid of the Dongshengmiao deposit is CO_2-rich (Editorial Committee of Mineral Deposits of China, 1989), which also characteristic of metamorphic fluid (Chen, 2006; Chen et al., 2007; Goldfarb et al., 2005; Pirajno, 2009). The fluid that remobilized Zn, Pb, and Cu was therefore derived from metamorphic devolatilization of the ore-hosting rocks, consistent with the synmetamorphic characteristic of Zn–Pb–Cu remobilization.

7. Conclusions

(1) Accompanying a Proterozoic rifting event, syngenetic mineralization took place, evidenced by the presence of pre-tectonic fine-grained pyrite, sulfides that are poor in radiogenic Pb, siderite layers, and B, Mn, P and Ba enriched layers with host rocks.
(2) Significant Zn–Pb–Cu remobilization formed as a result of metamorphic devolatilization of the ore-hosting rocks and contemporaneous thrust faulting. The synmetamorphic and syntectonic Zn–Pb–Cu remobilization took place in a metamorphic fluid, at a P–T range of greenschist facies metamorphism and a crustal depth of ~7–10 km. Sulfides were redistributed in shear structures or along grain boundaries of carbonate host rocks, and Fe-rich carbonates were favorite sinks for sulfide redistribution.
(3) The Early Cretaceous (ca. 136 Ma) regional metamorphism, thrust faulting, and consequent Zn–Pb–Cu remobilization took place during intraplate orogeny and crustal shortening.

Supplementary data to this article can be found online at http://dx.doi.org/10.1016/j.oregeorev.2014.06.015.

Acknowledgments

This study was financially supported by the National Basic Research Program of the People's Republic of China (2013CB429801) and the National Natural Science Foundation of China (40972057). We gratefully acknowledge the Zijin Mining Group Co. Ltd for the help during fieldwork. Dr. Bo Zhang and Mr. Guiming Shu were involved with SEM and electron microprobe analysis, respectively. Professors Richard Goldfarb, Paul Spry, Jinjiang Zhang and Chunjing Wei are thanked for offering us valuable suggestions on this study. Prof. Joël Brugger and Mr. Rodney Grapes assisted with the English language.

References

Cartwright, I., Oliver, N.H.S., 2000. Metamorphic fluids and their relationship to the formation of metamorphosed and metamorphogenic ore deposits. Rev. Econ. Geol. 11, 81–96.
Chen, Y.J., 2006. Orogenic-type deposits and their metallogenetic model and exploration potential. Geol. China 33, 1181–1196 (in Chinese with English abstract).
Chen, Y.J., Ni, P., Fan, H.R., Pirajno, F., Lai, Y., Su, W.C., Zhang, H., 2007. Diagnostic fluid inclusions of different types hydrothermal gold deposits. Acta Petrol. Sin. 23, 2085–2108 (in Chinese with English abstract).

Chiaradia, M., Schaltegger, U., Spiking, R., Wotzlaw, J., Ovtcharova, M., 2013. How accurately can we date the duration of magmatic-hydrothermal events in porphyry systems?—an invited paper. Econ. Geol. 108, 565–584.

Daoudene, Y., Ruffet, G., Cocherie, A., Ledru, P., Gapais, D., 2013. Timing of exhumation of the Ereendavaa metamorphic core complex (north-eastern Mongolia) – U–Pb and $^{40}Ar/^{39}Ar$ constraints. Journal of Asian Earth Sciences 62, 98–116.

Darby, B.J., Ritts, B.D., 2002. Mesozoic contractional deformation in the middle of the Asian tectonic collage: the intraplate Western Ordos fold–thrust belt, China. Earth Planet. Sci. Lett. 205, 13–24.

Darby, B.J., Ritts, B.D., 2007. Mesozoic structural architecture of the Lang Shan, North-Central China: intraplate contraction, extension, and synorogenic sedimentation. J. Struct. Geol. 29, 2006–2016.

Davis, G.A., Darby, B.J., 2010. Early Cretaceous overprinting of the Mesozoic Daqing Shan fold-and-thrust belt by the Hohhot metamorphic core complex, Inner Mongolia, China. Geosci. Front. 1, 1–20.

Davis, G.A., Wang, C., Zheng, Y.D., Zhang, J.J., Zhang, C.H., Gehrels, G.E., 1998. The enigmatic Yinshan fold-and-thrust belt of northern China: new views on its intraplate contractional styles. Geology 26, 43–46.

Ding, T.P., Jiang, S.Y., de Wan, F., Li, J.C., Song, B., Zhao, D.M., 1992. A Study on Stable Isotopes of Proterozoic Pb–Zn Mineral Belt in Northern China. Beijing Science and Technology Press, Beijing (127 pp.; in Chinese with English abstract).

Dong, S.W., Zhang, Y.Q., Chen, X.H., Long, C.X., Wang, T., Yang, Z.Y., Hu, J.M., 2008. The formation and deformational characteristics of East Asia multi-direction convergent tectonic system in Late Jurassic. Acta Geosci. Sin. 29, 306–317 (in Chinese with English abstract).

Editorial committee of Mineral Deposits of China, 1989. Mineral Deposits of China. Geological Publishing House, Beijing (in Chinese).

Gao, H.L., 2010. Structure Evolution and Chronology Constrains of Lang Shan in Neimeng Autonomous Region. China University of Geosciences, Beijing (74 pp. in Chinese with English abstract).

Goldfarb, R.J., Newberry, R.J., Pickthorn, W.J., Gent, C.A., 1991. Oxygen, hydrogen, and sulfur isotope studies in the Juneau gold belt, Southeastern Alaska: constraints on the origin of hydrothermal fluids. Econ. Geol. 86, 66–80.

Goldfarb, R.J., Baker, T., Dube, B., Groves, D.I., Hart, C.J.R., Gosselin, P., 2005. Distribution, character, and genesis of gold deposits in metamorphic terranes. Economic Geology, 100th Anniversary Volume, pp. 407–475.

Gu, L.X., Tang, X.Q., Wang, Z.J., Sun, Y., Wu, C.Z., Xiao, X.J., Ni, P., Wu, X.Y., 2004. Remobilisation experiment of chalcopyrite in massive sulphide ore by NaCl solution at 362 °C and a differential stress. Lithos 73, 47 (Suppl.).

Gu, L.X., Tang, X.Q., Wang, Z.J., Wu, C.Z., Lu, J.J., Ni, P., Wu, X., 2005. Sulphide remobilisation in NaCl solution at temperature of 362 °C under differential stress. Acta Petrol. Sin. 21, 1429–1434 (in Chinese with English abstract).

Gu, L.X., Zheng, Y.C., Tang, X.Q., Zaw, K., Della-Pasque, F., Wu, C.Z., Tian, Z.M., Lu, J.J., Ni, P., Li, X., Yang, F.T., Wang, X.W., 2007. Copper, gold and silver enrichment in ore mylonites within massive sulphide orebodies at Hongtoushan VHMS deposit, N.E. China. Ore Geol. Rev. 30, 1–29.

Han, B.F., Zhang, C., Zhao, L., Ren, R., Xu, Z., Chen, J.F., Zhang, L., Zhou, Y.Z., Song, B., 2010. A preliminary study of granitoids in western Inner Mongolia. Acta Petrol. Mineral. 29, 741–749 (in Chinese with English abstract).

Hatcher, R.D., 1995. Structural Geology: Principles, Concept, and Problems. Prentice Hall, New Jersey.

He, Z.J., Li, J.Y., Niu, B.G., Ren, J.S., 1998. A Late Jurassic intense thrusting-uplifting event in the Yanshan-Yinshan area, nothern China, and its sedimentary response. Geological Review 44, 407–417 (in Chinese with English abstract).

Hu, X., Gao, Q.W., Sun, G.Y., Lü, Y.F., 1981. A study on faults in the Dongshengmiao district, Bayannaoer League, Inner Mongolia. J. Shijiazhuang Univ. Econ. 4 (3), 31–93 (in Chinese).

Huang, W.X., 2009. Research on the Mine-forming Character of Polymetallic Sulfide Deposits in Langshan District, Proterozoic. Chengdu University of Technology, Chengdu (60 pp.; in Chinese with English abstract).

Huang, C.K., Bai, Z., Zhu, Y.S., Wang, H.Z., Shang, X.Z., 2001. Copper Deposit of China. Geological Publishing House, Beijing (in Chinese with English abstract).

Hutchison, M.N., Scott, S.D., 1981. Sphalerite geobarometry in the Cu–Fe–Zn–S system. Econ. Geol. 76, 143–153.

Leach, D.L., Hofstra, A.H., Church, S.E., Snee, L.W., B, V.R., E, Z.R., 1998. Evidence for Proterozoic and Late Cretaceous-Early Tertiary ore-forming events in the Coeur d'Alene district, Idaho and Montana. Economic Geology 93, 347–359.

Leach, D.L., Sangster, D.F., Kelley, K.D., Large, R.R., Garven, G., Allen, C.R., Gutzmer, J., Walters, S., 2005. Sediment-hosted lead–zinc deposits: a global perspective. Economic Geology, 100th Anniversary Volume, pp. 561–608.

Li, G., Liu, Z.H., 2009. Geological characteristics of Wengeng thrust fault in Langshan area of western Inner Mongolia. Global Geology 28, 451–459 (in Chinese with English abstract).

Li, Z.L., Xu, W.D., Pang, W.Z., 1986. S, Pb, C and O isotopic compositions and ore genesis of the stratabound polymetallic sulfide deposits in middle Inner Mongolia, China. Geochimica 1, 13–22 (in Chinese with English abstract).

Li, Q.L., Chen, F.K., Guo, J.H., Li, X.H., Yang, Y.H., Siebel, W., 2007. Zircon ages and Nd–Hf isotopic composition of the Zhaertai Group (Inner Mongolia): evidence for early Proterozoic evolution of the northern North China Craton. J. Asian Earth Sci. 30, 573–590.

Long, L.Z., 2009. Geological Characteristics and Genesis Analysis of Dongshenmiao Lead–Zinc Ore Deposit in the Inner Mongolia. Central South University (in Chinese with English abstract).

Ludwig, K.R., 2003. User's Manual for Isoplot 3.00: A Geochronological Toolkit for Microsoft Excel (74 pp.).

Marshall, B., Vokes, F.M., Larocque, A.C.L., 2000. Regional metamorphic remobilisation: upgrading and formation of ore deposits. In: Spry, P.G., Marshall, B., Vokes, F.M. (Eds.), Metamorphosed and metamorphogenic ore deposits. Reviews in Economic Geology, 11, pp. 19–38.

McDougall, I., Harrison, T.M., 1999. Geochronology and Thermochronology by the $^{40}Ar/^{39}Ar$ Method. Oxford University Press, New York.

Miyashiro, A., 1994. Metamorphic Petrology. University College London Press, London.

Niu, S.Y., Xu, C.S., Hu, X., Sun, A.Q., 1991. A study of ore-control structure in the Langshan Mountain area, Inner Mongolia. J. Changchun Univ. Earth Sci. 21, 313–320 (in Chinese with English abstract).

Passchier, C.W., Trouw, R.A.J., 2005. Microtectonics. Springer, Berlin.

Peng, R.M., Zhai, Y.S., 1997. The confirmation of the metamorphic double-peaking volcanic rocks in Langshan Group of the Dongshengmiao ore district, Inner Mongolia and its significance. Earth Sci. J. China Univ. Geosci. 22, 589–594 (in Chinese with English abstract).

Peng, R.M., Zhai, Y.S., 2004. The characteristics of hydrothermal exhalative mineralization of the Langshan–Zhaertai belt, Inner Mongolia, China. Earth Sci. Front. 11, 257–268 (in Chinese with English abstract).

Peng, R.M., Zhai, Y.S., Wang, Z.G., 2000. Ore-controlling synchronous faults of Mesoproterozoic Dongshengmiao and Jiashengpan SEDEX-type ore deposits, Inner Mongolia. Earth Sci. J. China Univ. Geosci. 4, 404–410 (in Chinese with English abstract).

Peng, R.M., Zhai, Y.S., Han, X.F., Wang, J.P., Wang, Z.G., Qin, J.W., 2007a. Magmatic hydrothermal overprinting in the Mesoproterozoic Dongshengmiao deposit, Inner Mongolia: geological and fluid inclusion evidences. Acta Petrol. Sin. 23, 145–152 (in English).

Peng, R.M., Zhai, Y.S., Han, X.F., Wang, Z.G., Wang, J.P., Shen, C.L., Chen, X.F., 2007b. Mineralization respond to the structural evolution in the Langshan orogenic belt, Inner Mongolia. Acta Petrol. Sin. 23, 679–688 (in Chinese with English abstract).

Peng, R.M., Zhai, Y.S., Chen, X.F., Liu, Q., Lv, J.Y., Shi, Y.X., Wang, G., Li, S.B., Wang, L.G., Ma, Y.T., Zhang, P., 2010. Discovery of Neoproterozoic acid volcanic rock in the southwestern section of Langshan, Inner Mongolia. Chin. Sci. Bull. 55, 2611–2620 (in Chinese with English abstract).

Pi, Q.H., Liu, C.Z., Chen, Y.L., Li, Y.Q., Li, D.P., 2010. Formation epoch and genesis of intrusive rocks in Huogeqi orefield of Inner Mongolia and their relationship with copper mineralization. Mineral Deposits 29, 437–451 (in Chinese with English abstract).

Pirajno, F., 2009. Hydrothermal Processes and Mineral Systems. Springer.

Qi, G.W., Zhang, J.J., Wang, X.S., Guo, L., 2007. Mesozoic thrusts and extensional structures in the Daqingshan orogen, Inner Mongolia, and their temporal and spatial relationship. Prog. Nat. Sci. 17, 177–186 (in Chinese with English abstract).

Rui, Z.Y., Shi, L.D., Fang, R.H., 1994. Geology of Nonferrous Metallic Deposits in the Northern Margin of the North China Landmass and Its Adjacent Area. Geological Publishing House, Beijing (in Chinese with English abstract).

Singer, D.A., 1995. World class base and precious metal deposits—a quantitative analysis. Econ. Geol. 90, 88–104.

Stacey, J.S., Kramers, J.D., 1975. Approximation of terrestrial lead isotope evolution by a two-stage model. Earth Planet. Sci. Lett. 26, 207–221.

Sun, A.Q., Niu, S.Y., 1994. Structure control on mineralization and prognosis in the Dongshengmiao troilite mine. Geol. Explor. Nonferrous Met. 3, 146–150 (in Chinese with English abstract).

Sun, L.X., Zhao, F.Q., Wang, H.C., Ren, B.F., Peng, S.H., Teng, F., 2013. Zircon U–Pb geochronology of metabase rocks from the Baoyintu Block in the Langshan area, Inner Mongolia, and is tectonic significance. Acta Geol. Sin. 87, 197–207 (in Chinese with English abstract).

Suo, W., 1992. Characteristics and genesis of thrust faults in the Dongshengmiao mining area, Inner Mongolia. Geol. Chem. Miner. 14, 50 (in Chinese).

Wang, T., Zheng, Y.D., Li, T.B., Gao, Y.J., 2004. Mesozoic granitic magmatism in extensional tectonics near the Mongolian border in China and its implications for crustal growth. J. Asian Earth Sci. 23, 715–729.

Wulatehouqi Zijin Mining Group Co. Ltd, 2008. Report of Exploration on the Sanguikou South Ore Belt of the Dongshengmiao deposit, Wulatehouqi, Inner Mongolia (in Chinese).

Xiao, W.J., Windley, B.F., Hao, J., Zhai, M.G., 2003. Accretion leading to collision and the Permian Solonker suture, Inner Mongolia, China: termination of the central Asian orogenic belt. Tectonics 22, 1069–1089.

Xu, Z.Y., Liu, Z.H., Yang, Z.S., 2001. Mesozoic orogenic movement and tectonic evolution in Daqingshan region, Inner Mongolia. J. Changchun Univ. Sci. Technol. 31, 317–322 (in Chinese with English abstract).

Xu, B., Charvet, J., Chen, Y., Zhao, P., Shi, G.Z., 2013. Middle Paleozoic convergent orogenic belts in western Inner Mongolia (China): framework, kinematics, geochronology and implications for tectonic evolution of the Central Asian Orogenic Belt. Gondwana Res. 23, 1342–1364.

Yakubchuk, A., 2004. Architecture and mineral deposit settings of the Altaid orogenic collage: a revised model. J. Asian Earth Sci. 23, 761–779.

Yang, J.P., 1992. The origin and the ore fabric property of the bedded lead–zinc (copper) sulfide deposit in Dong Sheng Miao, Inner Mongolia. J. Heibei Coll. Geol. 5, 489–552 (in Chinese with English abstract).

Yang, F.X., 1998. Characteristics of mylonites in the Langshan district and its tectonic implications. Northwest. Geol. 79, 1–7 (in Chinese).

Zhai, Y.S., Peng, R.M., Chen, C.X., Cai, K.Q., Deng, J., Chen, X.M., Cheng, X.J., Wang, J.P., 2008. Genesis and Structure of Major Metallogenic Series of China. Geological Publishing House, Beijing (in Chinese with English abstract).

Zhang, J.J., Qi, G.W., Guo, L., Liu, J., 2009a. ^{40}Ar–^{39}Ar dating of the Mesozoic thrusting in Daqingshan thrust–nappe system, Inner Mongolia, China. Acta Petrol. Sin. 25, 609–620 (in Chinese with English abstract).

Zhang, S.H., Zhao, Y., Song, B., Hu, J.M., Liu, S.W., Yang, Y.H., Chen, F.K., Liu, X.M., Liu, J., 2009b. Contrasting Late Carboniferous and Late Permian–Middle Triassic intrusive

suites from the northern margin of the North China craton: geochronology, petrogenesis, and tectonic implications. Geol. Soc. Am. Bull. 121, 181–200.
Zhang, S.H., Zhao, Y., Liu, J.M., Hu, J.M., Song, B., Liu, J., Wu, H., 2010a. Geochronology, geochemistry and tectonic setting of the Late Paleozoic–Early Mesozoic magmatism in the northern margin of the North China Block: a preliminary review. Acta Petrol. Mineral. 29, 824–842 (in Chinese with English abstract).
Zhang, Z.B., Li, J.H., Huang, C.Y., Liu, H., Zhao, Y.H., 2010b. Study on genesis and ore prospecting of Dongshengmiao deposit in Inner Mongolia. J. Jilin Univ. (Earth Sci. Ed.) 40, 791–800 (in Chinese with English abstract).
Zheng, Y.D., Davis, G.A., Wang, C., Darby, B.J., Hua, Y.G., 1998. Major thrust sheet in the Daqing Shan Mountains, Inner Mongolia, China. Sci. China Ser. D Earth Sci. 41, 553–560.
Zhong, R.C., Li, W.B., Chen, Y.J., Huo, H.L., 2012. Ore-forming conditions and genesis of the Huogeqi Cu–Pb–Zn–Fe deposit in the northern margin of the North China Craton: evidence from ore petrologic characteristics. Ore Geol. Rev. 44, 107–120.
Zhong, R.C., Li, W.B., Chen, Y.J., Yue, D.C., Yang, Y.F., 2013. P–T–X conditions, origin, and evolution of Cu-bearing fluids of the shear zone-hosted Huogeqi Cu–(Pb–Zn–Fe) deposit, northern China. Ore Geol. Rev. 50, 83–97.